# ChemComm

Chemical Communications

ROYAL SOCIETY
OF CHEMISTRY

**COMMUNICATION**
Jonathan A. Foster *et al.*
Liquid exfoliation of alkyl-ether functionalised layered metal–organic frameworks to nanosheets

175 YEARS

# Liquid exfoliation of alkyl-ether functionalised layered metal–organic frameworks to nanosheets†

Jonathan A. Foster,*[a] Sebastian Henke,[b] Andreas Schneemann,[b] Roland A. Fischer[cd] and Anthony K. Cheetham[e]

We report the synthesis of a 2D-layered metal–organic framework incorporating weakly interacting chains designed to aid exfoliation of the layers into nanosheets. Dispersion of the nanosheets exposes labile metal-sites which are shown to exchange solvent molecules allowing the nanosheets to act as sensors in suspension.

The liquid exfoliation of layered materials into two-dimensional nanosheets has attracted much recent attention, most prominently with graphene but also many other layered oxides, clays and organic polymers.[1–4] Metal–organic frameworks (MOFs) combine the tunability of organic linkers with the unique properties of metal ions allowing the creation of diverse, well defined architectures with tailored properties.[5–8] This flexibility has allowed them to be developed for applications as diverse as 'smart' materials and sensors to light harvesting, gas storage and drug delivery.[6,9] Despite the large number of layered MOFs in the literature, only a small number of examples of metal–organic framework nanosheets (MONs) have so far been reported.[10–22]

A number of methods for the exfoliation of layered materials have been developed, most straight forwardly in the case of neutral layered MOFs by the use of ultrasound to preferentially break apart weaker interactions between layers in the structures.[15–22] MONs based on the robust metal-paddle wheel (PW) secondary building unit were some of the first to be exfoliated to form nano-sheets.[10,18,19] The Fischer group have previously reported a series of 1,4-benzenedicarboxylate derived linkers functionalised with a range of different short chains which can adopt a number of MOF structures.[23–26] Here we report the first in a new series of layered MOFs based on the PW motif incorporating akyl-ether functional groups which we hypothesised would be positioned between the layers, aiding exfoliation and interacting with solvent molecules to enhance dispersion.

Furthermore, exfoliation of the frameworks opens up access to the labile coordination sites at the axial positions of the PWs which would otherwise be buried within the densely packed MOF structure. MOFs with labile metal-sites are of particular interest owing to their potential as catalysts and sensors and 2D nanosheets are ideal for such applications owing to their large surface areas and the periodic array of active sites they present.[27] We investigate the effect of different coordinating solvents on the MOF structure and calculate the binding constant of pyridine to a suspension of nanosheets through a UV-vis spectroscopic titration.

2,5-Bis(3-methoxypropoxy)-1,4-benzenedicarboxylate, compound $H_2(1)$,[28] was synthesised *via* Williamson etherification of dimethyl 2,5-dihydroxy-1,4-benzenedicarboxylate with 1-bromo-3-methoxy-propane.[25] Heating of $H_2(1)$ with copper nitrate in DMF in a sealed reaction vial at 110 °C for 18 h resulted in the formation of a green microcrystalline powder. When the synthesis was repeated using zinc nitrate in place of copper nitrate, clear cubic crystals were obtained which were identified as Zn(1)(DMF) by single crystal X-ray diffraction (Fig. 1). The framework crystallises in the triclinic space group *P*1 with the expected PW building units. Four carboxylate linkers **1** coordinate to the $Zn_2$-paddlewheel and interconnect these units in the two-dimensional **sql** topology,[29] while DMF coordinates to the axial sites of the PWs. Hence, the lamellar structure features strong metal-carboxylate bonding within the layers and weakly interacting 3-methoxypropoxy groups between the layers.

Analysis (Pawley refinement) of the X-ray powder diffraction pattern (XRPD) of the copper derivative Cu(1)(DMF) clearly indicates the material is isostructural with Zn(1)(DMF) (ESI,† Section S3.3). Small differences in the unit cell parameters (ESI,† Table S2) are ascribed to the different ionic radii and

[a] *University of Sheffield, Department of Chemistry, Sheffield, S3 7HF, UK.*
   *E-mail: Jona.foster@sheffield.ac.uk*
[b] *Lehrstuhl für Anorganische Chemie II, Organometallics & Materials,*
   *Ruhr-Universität Bochum, Germany*
[c] *Department of Chemistry, Technical University Munich, Lichtenbergstrasse 4,*
   *D-85748 Garching, Germany*
[d] *Catalysis Research Centre, Technical University Munich,*
   *Ernst-Otto-Fischer Strasse 1, 85748 Garching, Germany*
[e] *University of Cambridge, Materials Science and Metallurgy,*
   *27 Charles Babbage Road, Cambridge, CB3 0FS, UK.*

† Electronic supplementary information (ESI) available: Ligand and MOF synthesis, description of crystal structure, refinement and PXRD analysis, additional AFM images, binding isotherms. CCDC 1460747. For ESI and crystallographic data in CIF or other electronic format see DOI: 10.1039/c6cc05154e
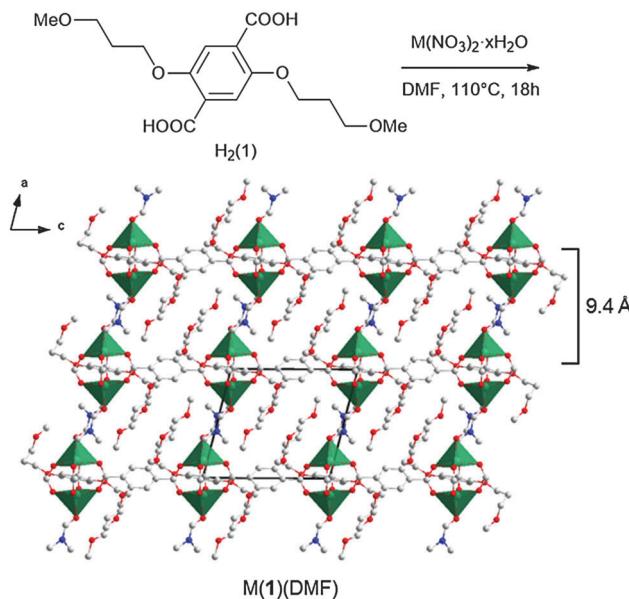
**Fig. 1** Reaction scheme for the synthesis of M(**1**)(DMF) (with M = Cu, Zn) showing the crystal structure of Zn(**1**)(DMF) viewed along the *b*-axis highlighting the lamellar structure with an interlayer spacing of ∼9.4 Å (∼9.6 Å for Cu(**1**)(DMF)). C, N and O atoms are shown in grey, blue and red. The coordination polyhedra of the M ions are displayed in green. H atoms have been omitted for clarity.



**Fig. 2** (a) Images showing a suspension of Cu(**1**) nanosheets in DMF with characteristic Tyndall Scattering of laser light. AFM images and height profiles corresponding to blue lines for nanosheets formed by exfoliation of (b) Zn(**1**) in DMF (c) Cu(**1**) in H$_2$O.

different ligand field effects of Zn$^{2+}$ and Cu$^{2+}$. XRPD analysis of a bulk sample of Zn(**1**)(DMF) revealed a second phase which was identified as the previously reported[23] 3D cubic Zn$_4$O(**1**)$_3$ framework structure (isoreticular to MOF-5).[30]

The frameworks were sonicated in DMF with a concentration of 1 mg mL$^{-1}$ for 30 minutes and the resulting suspension was centrifuged at 1500 rpm for 45 minutes to remove larger particles. The supernatant appeared clear but showed evidence of Tyndall scattering when irradiated with a laser (Fig. 2a) indicating the formation of a fine suspension. The supernatant was deposited onto a quartz crystal and imaged using atomic force microscopy (AFM) to reveal nanosheets with thicknesses ranging from 5–30 nm and lateral dimensions between 100–500 nm (Fig. 2b and ESI,† Section S4). The crystal structure of Zn(**1**)(DMF) predicts a single layer thickness of approx. 14.5 Å and a shorter interlayer spacing of approx. 9.4 Å (due to interpenetration of the 3-methoxypropoxy groups). This indicates a minimum thickness of the nanosheets corresponding to approximately 5 MOF layers, comparable to those observed for related PW based MONs.[19]

The MONs were isolated by centrifugation of the suspensions at 4000 rpm for 30 minutes after which no Tyndall Scattering was observed in the remaining solutions. XRPD patterns of concentrated suspensions of the nanosheets measured using Kapton capillaries showed that the material matched that of the bulk material indicating no structural rearrangements had taken place (Fig. 3b and c). It is worth noting that no systematic broadening of the peaks in the XRPD pattern resulting from the reduced dimensions of the nanosheets are observed; this may be due to the dominant contributions of larger crystalline particles or indicate restacking of the MONs in the concentrated suspension.
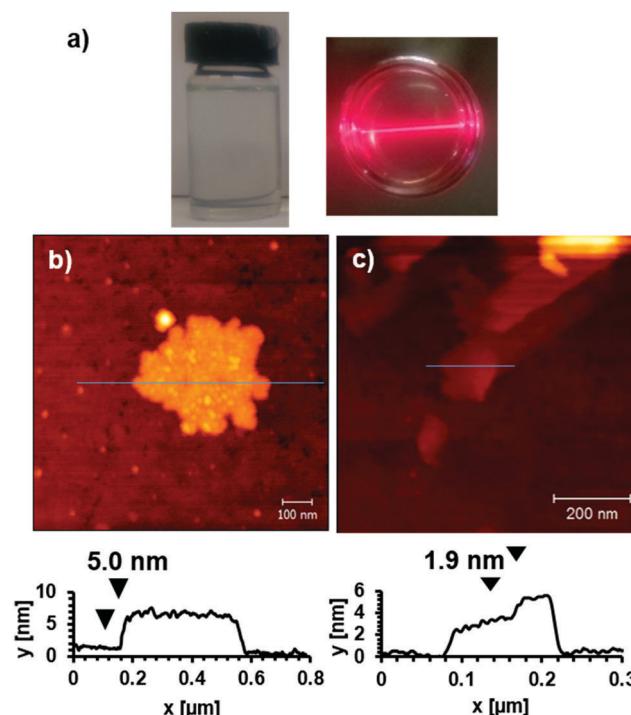
The incorporation of akyl-ether linkages into the frameworks was intended to aid their dispersion into aqueous suspensions. The exfoliation of Cu(**1**)(DMF) into water was therefore investigated using the protocol previously described. AFM images of the MONs deposited from aqueous suspensions onto quartz showed typical thicknesses ranging from 2–30 nm and lateral dimensions between 50–500 nm (Fig. 2c). XRPD patterns (Fig. 3e) indicate the formation of a distinct pattern which could be indexed and refined in the tetragonal space group $I4_1cd$ (ESI,† Section S3.3). The new phase is ascribed to the exchange of DMF at the axial sites of the PWs against the smaller water molecule, to yield Cu(**1**)(H$_2$O), which features a different stacking of the layers. Unfortunately, *ab initio* structure solution from the XRPD patterns was unsuccessful due to the complexity of the organic linker with flexible substituents. However, space group symmetry and unit cell dimensions clearly indicate that the 2D **sql** topology of the framework is maintained. The space group further suggests the presence of four layers in the unit cell, which are arranged in a staggered arrangement (ESI,† Fig. S20). Consequently the interlayer distance is only ∼7.8 Å for Cu(**1**)(H$_2$O) compared to ∼9.6 Å for Cu(**1**)(DMF).

Cu(**1**)(DMF) was exfoliated into DMF–water mixtures (50%, 25%, 10% and 1% DMF by volume). Analysis of the resulting XRPD patterns shows a gradual transition from the triclinic Cu(**1**)(DMF) structure to the tetragonal Cu(**1**)(H$_2$O) structure with a mixture of the two phases observed in 10% DMF:water (Fig. 3d, see ESI,† for details). Samples initially exfoliated in water, were collected by centrifugation and redispersed in DMF. XRPD patterns showed complete conversion back to the DMF
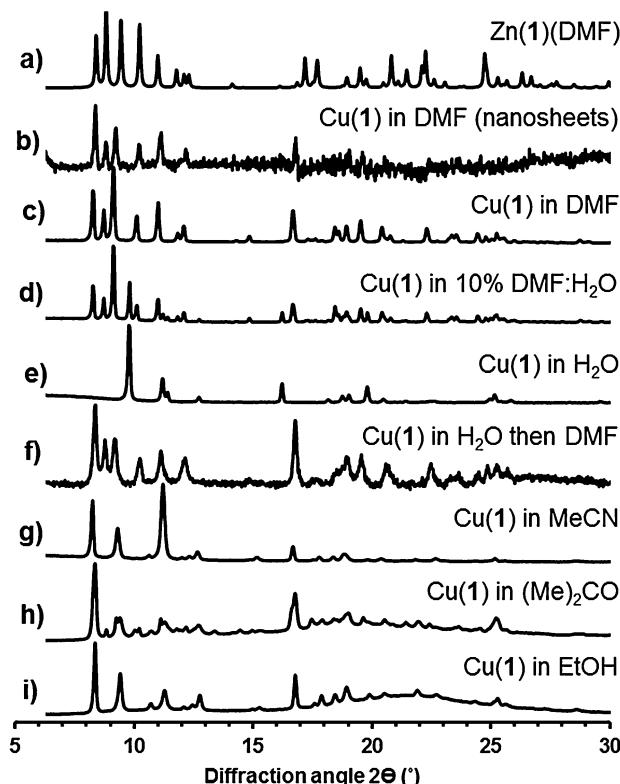
Fig. 3 (a) Calculated XRPD pattern for Zn(**1**)(DMF). Experimental XRPD patterns for (b) nanosheets of Cu(**1**) exfoliated in DMF*[#], solids collected following exfoliation of Cu(**1**)(DMF) in (c) DMF, (d) 10% DMF–water, (e) water, (f) water, followed by reimersion in DMF for 4 days*[#], (g) acetonitrile, (h) acetone*, and (i) ethanol*. Patterns marked with an * were measured using Kapton capillaries to prevent solvent loss, those with a [#] are background subtracted patterns, other measurements were collected using dried powders on flat substrates.

structure over 4 days (Fig. 3f) when the DMF was repeatedly changed. These results indicate that the lamellar PW structure is retained in aqueous suspensions with coordinated DMF molecules at the axial position exchanging with smaller $H_2O$ molecules to give Cu(**1**)($H_2O$).

The exfoliation of Cu(**1**)(DMF) into other coordinating solvents was also investigated. XRPD patterns for Cu(**1**)(DMF) exfoliated into acetonitrile, acetone and ethanol (Fig. 3g–i) could all be indexed in a triclinic cell similar to that of Cu(**1**)(DMF) but with shorter interlayer distance and smaller unit cell volume.

The metrics of the unit cell further give a clear indication of a slipping of the layers with respect to the original Cu(**1**)(DMF) phase (see ESI,† for details). Samples exfoliated into acetone showed a mixture of the new phase and the original Cu(**1**)(DMF) material. IR patterns for the samples derived from acetone, ethanol and acetonitrile matched closely and no peaks corresponding to the relevant solvent molecules could be identified (ESI,† Fig. S21). Likewise, thermogravimetric analysis (TGA) of these three samples showed no significant weight loss corresponding to solvent removal upon heating the samples up to 260 °C (ESI,† Fig. S22). Contrary, for Cu(**1**)(DMF) and Cu(**1**)($H_2O$) solvent loss was observed upon heating to 260 °C. On the basis of these observations, we suggest that the phases derived from

acetone, ethanol and acetonitrile are identical and exhibit the formula Cu(**1**). We propose that in these structures the methoxy-oxygen atoms of the flexible 3-methoxypropoxy chains intramolecularly (or intermolecularly) coordinate to the PW in place of more weakly coordinating, volatile solvent molecules (MeCN, (Me)$_2$CO or EtOH). Similar side group effects have been proposed for IRMOFs featuring flexible, methoxy-terminated substituents.[23] High resolution synchrotron data are required to undertake detailed structural studies on these materials but it is useful to highlight the strong effect of exfoliation into different solvents on the MON structure which has not been documented in other studies on MOF nanosheets.

The photophysical properties and large surface area of the nanosheets in aqueous suspension were exploited to act as sensors for the detection of a model guest compound, pyridine. Related MONs have previously been shown to function as sensors for ethylamine when coated on a surface,[18] but here we show they can be used in suspension and are able to quantify the binding interaction. A calibration curve, obtained by serial dilution of a suspension containing a known mass of Cu(**1**)(DMF), was used to estimate the concentration of the nanosheets in aqueous suspension as 0.55 mg mL$^{-1}$ or 1.16 mM based on the relative molecular mass of the starting material (ESI,† Fig. S28).[4] This compares with estimations of the concentration of nanosheets following exfoliation in DMF of 0.02 mg mL$^{-1}$ for Cu(**1**)(DMF) and 0.11 mg mL$^{-1}$ for Zn(**1**)(DMF) calculated using the same method.

Aliquots of a solution of pyridine in the host suspension (0.22 mM) were titrated into freshly diluted aqueous suspensions of nanosheets (0.29 mM) and monitored by UV-vis spectroscopy. Addition of pyridine resulted in a bathochromic shift in the $\lambda_{max}$ of the adsorption band of the MONs from 302–306 nm and a 1.5 fold increase in absorption intensity (Fig. 4). This data was used to calculate a binding constant for pyridine to the nanosheets in water as $K_a = 30 \pm 8$ M$^{-1}$. These changes are consistent with the expected substitution of water molecules for pyridine at the axial position of the copper PWs resulting in changes in the absorption band of the coordinated functionalised dicarboxylate **1**.[31]
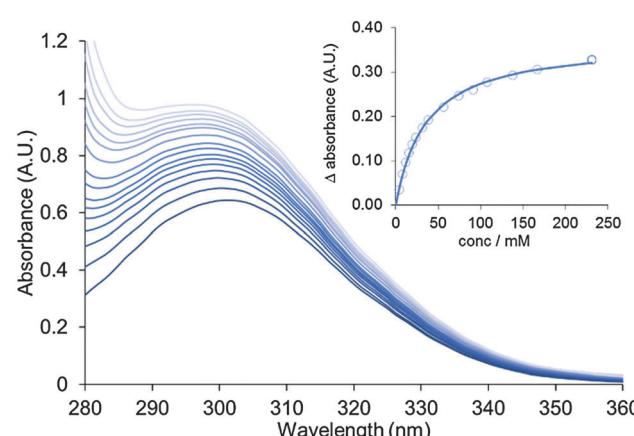


Fig. 4 UV-vis titration showing addition of aliquots of a pyridine solution to an aqueous suspension of Cu(**1**) nanosheets. Inset shows a plot of change in absorbance against concentration of pyridine which is fitted to calculate the binding constant for pyridine to the nanosheets ($K_a = 30 \pm 8$ M$^{-1}$).

In summary, we have demonstrated how ultrasound can be used to exfoliate layered copper and zinc based metal–organic frameworks functionalised with flexible methoxy-terminated side chains to produce suspensions of nanosheets in a range of solvents. Exfoliation of the nanosheets exposes labile metal-sites which are shown to exchange solvent molecules inducing photophysical changes which allow for the sensing of pyridine. This study represents the first in a potentially large series of metal–organic framework nanosheets in which different functionalities are introduced to the nanosheets surface to aid exfoliation and facilitate sensing or catalysis.

## Notes and references

1 V. Nicolosi, M. Chhowalla, M. G. Kanatzidis, M. S. Strano and J. N. Coleman, *Science*, 2013, **340**, 1226419.
2 R. Mas-Balleste, C. Gomez-Navarro, J. Gomez-Herrero and F. Zamora, *Nanoscale*, 2011, **3**, 20–30.
3 X. Zhang and Y. Xie, *Chem. Soc. Rev.*, 2013, **42**, 8187–8199.
4 J. N. Coleman, M. Lotya, A. O'Neill, S. D. Bergin, P. J. King, U. Khan, K. Young, A. Gaucher, S. De, R. J. Smith, I. V. Shvets, S. K. Arora, G. Stanton, H.-Y. Kim, K. Lee, G. T. Kim, G. S. Duesberg, T. Hallam, J. J. Boland, J. J. Wang, J. F. Donegan, J. C. Grunlan, G. Moriarty, A. Shmeliov, R. J. Nicholls, J. M. Perkins, E. M. Grieveson, K. Theuwissen, D. W. McComb, P. D. Nellist and V. Nicolosi, *Science*, 2011, **331**, 568–571.
5 H. C. Zhou, J. R. Long and O. M. Yaghi, *Chem. Rev.*, 2012, **112**, 673–674.
6 H. Furukawa, K. E. Cordova, M. O'Keeffe and O. M. Yaghi, *Science*, 2013, **341**, 1230444.
7 F. A. A. Paz, J. Klinowski, S. M. F. Vilela, J. P. C. Tome, J. A. S. Cavaleiro and J. Rocha, *Chem. Soc. Rev.*, 2012, **41**, 1088–1110.
8 S. M. Cohen, *Chem. Rev.*, 2012, **112**, 970–1000.
9 A. Schneemann, S. Henke, I. Schwedler and R. A. Fischer, *ChemPhysChem*, 2014, **15**, 823–839.
10 T. Rodenas, I. Luz, G. Prieto, B. Seoane, H. Miro, A. Corma, F. Kapteijn, I. X. F. X. Llabres and J. Gascon, *Nat. Mater.*, 2015, **14**, 48–55.
11 C. Marti-Gastaldo, J. E. Warren, K. C. Stylianou, N. L. O. Flack and M. J. Rosseinsky, *Angew. Chem., Int. Ed.*, 2012, **51**, 11044–11048.
12 S. C. Junggeburth, L. Diehl, S. Werner, V. Duppel, W. Sigle and B. V. Lotsch, *J. Am. Chem. Soc.*, 2013, **135**, 6157–6164.
13 A. Gallego, C. Hermosa, O. Castillo, I. Berlanga, C. J. Gomez-Garcia, E. Mateo-Marti, J. I. Martinez, F. Flores, C. Gomez-Navarro, J. Gomez-Herrero, S. Delgado and F. Zamora, *Adv. Mater.*, 2013, **25**, 2141–2146.
14 T. Araki, A. Kondo and K. Maeda, *Chem. Commun.*, 2013, **49**, 552–554.
15 J.-C. Tan, P. J. Saines, E. G. Bithell and A. K. Cheetham, *ACS Nano*, 2012, **6**, 615–621.
16 P. J. Saines, M. Steinmann, J.-C. Tan, H. H. M. Yeung, W. Li, P. T. Barton and A. K. Cheetham, *Inorg. Chem.*, 2012, **51**, 11198–11209.
17 Y. Peng, Y. Li, Y. Ban, H. Jin, W. Jiao, X. Liu and W. Yang, *Science*, 2014, **346**, 1356–1359.
18 Z.-Q. Li, L.-G. Qiu, W. Wang, T. Xu, Y. Wu and X. Jiang, *Inorg. Chem. Commun.*, 2008, **11**, 1375–1377.
19 P. Z. Li, Y. Maeda and Q. Xu, *Chem. Commun.*, 2011, **47**, 8436–8438.
20 A. Kondo, C. C. Tiew, F. Moriguchi and K. Maeda, *Dalton Trans.*, 2013, **42**, 15267–15270.
21 P. J. Beldon, S. Tominaka, P. Singh, T. S. Dasgupta, E. G. Bithell and A. K. Cheetham, *Chem. Commun.*, 2014, **50**, 3955–3957.
22 P. Amo-Ochoa, L. Welte, R. Gonzalez-Prieto, P. J. Sanz Miguel, C. J. Gomez-Garcia, E. Mateo-Marti, S. Delgado, J. Gomez-Herrero and F. Zamora, *Chem. Commun.*, 2010, **46**, 3262–3264.
23 S. Henke, R. Schmid, J.-D. Grunwaldt and R. A. Fischer, *Chem. – Eur. J.*, 2010, **16**, 14296–14306.
24 S. Henke, A. Schneemann, S. Kapoor, R. Winter and R. A. Fischer, *J. Mater. Chem.*, 2012, **22**, 909–918.
25 S. Henke, A. Schneemann, A. Wütscher and R. A. Fischer, *J. Am. Chem. Soc.*, 2012, **134**, 9464–9474.
26 I. Schwedler, S. Henke, M. T. Wharmby, S. R. Bajpe, A. K. Cheetham and R. A. Fischer, *Dalton Trans.*, 2016, **45**, 4230–4241.
27 J. Liu, L. Chen, H. Cui, J. Zhang, L. Zhang and C.-Y. Su, *Chem. Soc. Rev.*, 2014, **43**, 6011–6061.
28 S. Henke and R. A. Fischer, *J. Am. Chem. Soc.*, 2011, **133**, 2064–2067.
29 M. O'Keeffe, M. A. Peskov, S. J. Ramsden and O. M. Yaghi, *Acc. Chem. Res.*, 2008, **41**, 1782–1789.
30 H. Li, M. Eddaoudi, M. O'Keeffe and O. M. Yaghi, *Nature*, 1999, **402**, 276–279.
31 B. Supronowicz, A. Mavrandonakis and T. Heine, *J. Phys. Chem. C*, 2015, **119**, 3024–3032.